Supplementary Figures 1-8 and Supplementary Table 1

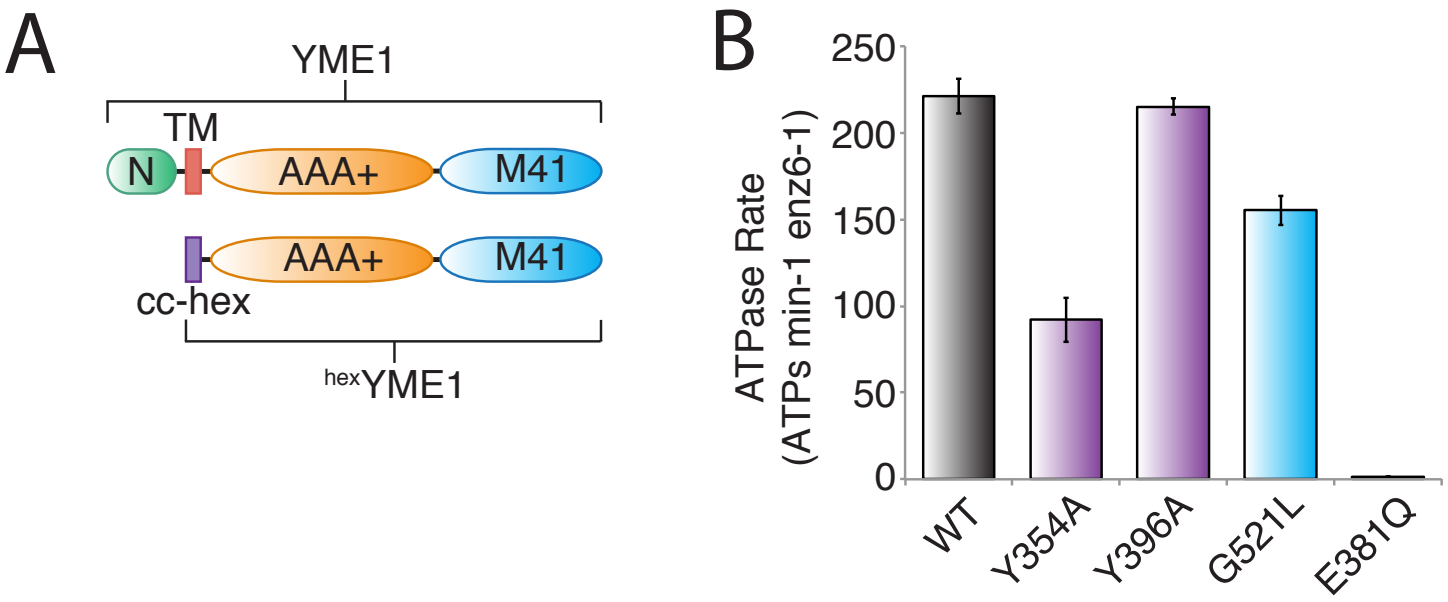

Supplementary Figure 1. Hex YME1 purification and ATPase activity validation

A) Schematic of the ^{hex}YME1 construct compared to full-length YME1. **B)** ATP hydrolysis rates for all variants of ^{hex}YME1 used in this study. Mutation of pore loop 1 Tyr354 to Alanine yields ~40% of the wild-type rate, whereas no decrease is seen for the mutation of pore loop 2 Tyr396 to Alanine. Mutation of Gly521L to Leucine yields ~70% of the wild-type rate and close to no ATP hydrolysis is observed for the mutation of the Walker-B Glu381 to Glutamine.

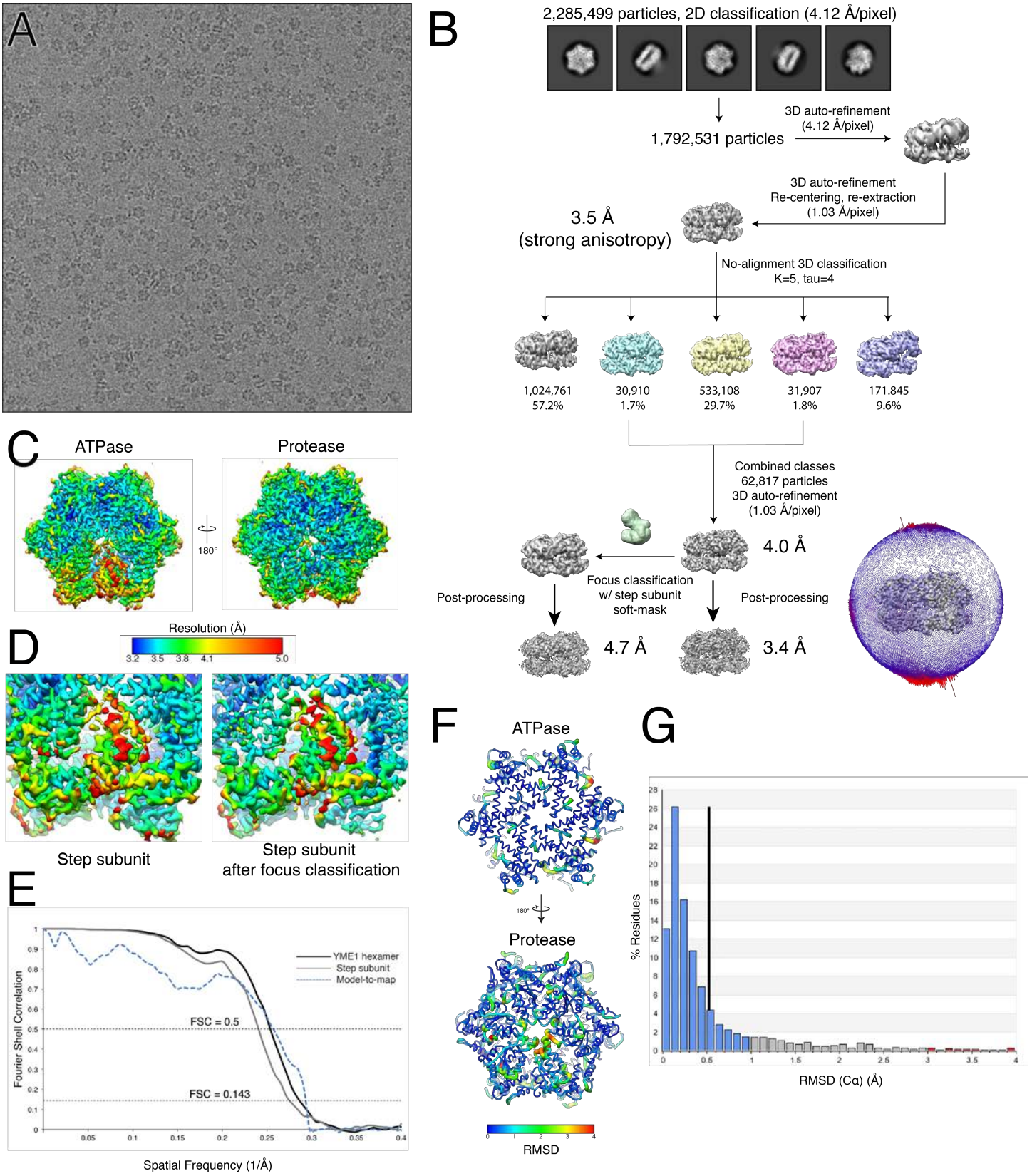

Supplementary Figure 2. Validation of the structural data

A) Representative cryo-EM micrograph showing the quality of the raw data collected and used to generate the 3D reconstruction of substrate bound ^{hex}YME1^{WB}. **B)** Processing scheme followed using the RELION software (Scheres 2012) to obtain the final 3D reconstructions of substrate bound ^{hex}YME1^{WB} from cryo-EM data. The

final Euler distribution of the 62,817 particles used for the final reconstruction is shown in the lower right. **C)** Local resolution were calculated using BSOFT (Cardone 2013), showing that the final EM-density of YME1 shows the resolution varies from 3.2 Å at the core of the complex to >5 Å for certain parts of the step subunit. **D)** Comparison of the local resolution for the step subunit before and after 3D focused classification reveals significant improvements that enabled atomic modeling of this subunit. **E)** Fourier Shell Correlation (FSC) of the full YME1 hexamer (black line), the step subunit after focused reconstruction (gray line) and the top-refined atomic model vs. the full YME1 map (dotted blue). **F)** Worm representation, colored according to the per-residue Cα RMSD values (in Å) determined from ten equally representative atomic models (Herzik 2017). **G**) Histogram of the per-residue Cα RMSD values calculated from the top 10 refined atomic models with the mean per-residue Cα RMSD value shown as a black vertical bar.

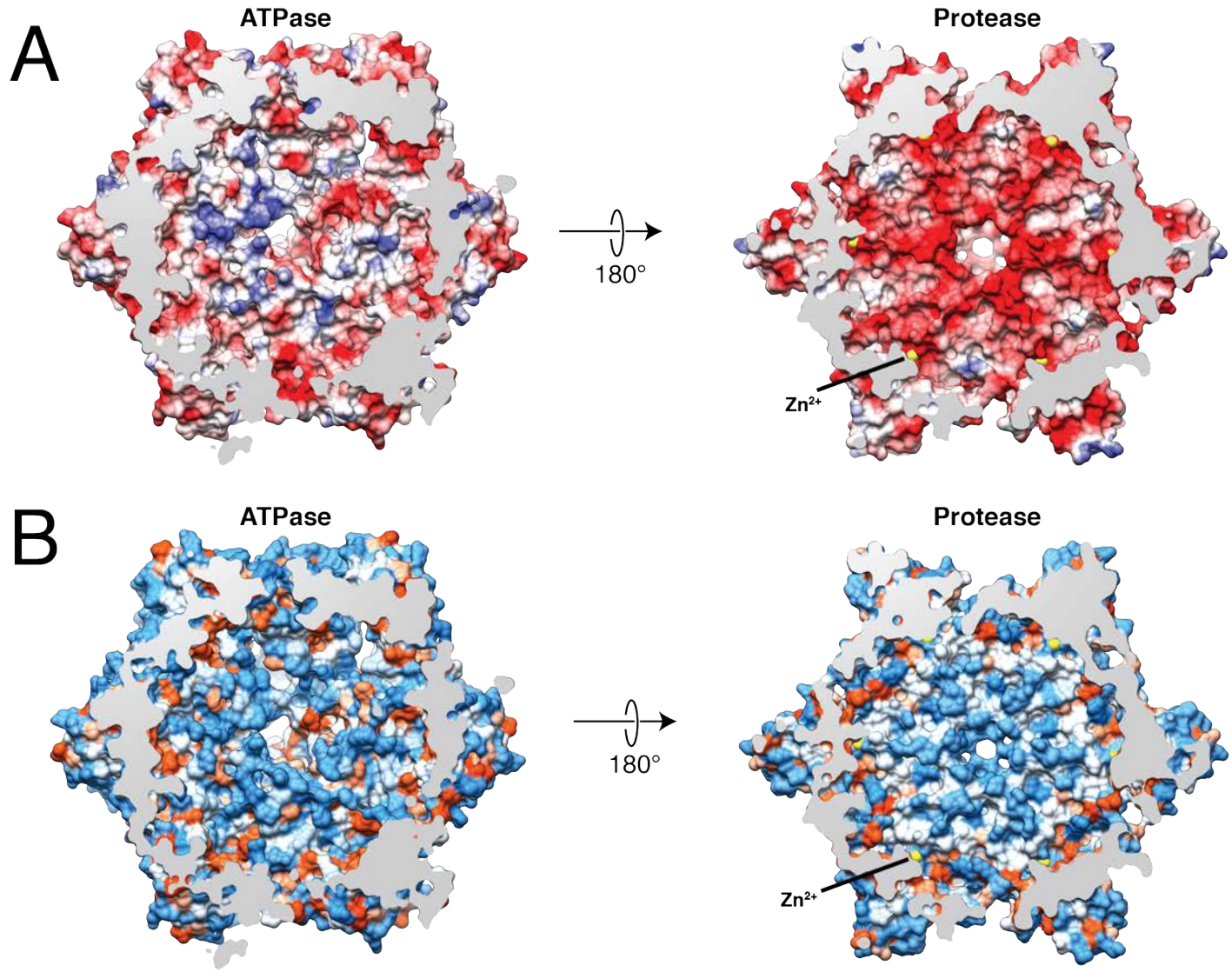
A
ATPase
Protease
180°
Zn2+
B
ATPase
Protease
180°
Zn2+

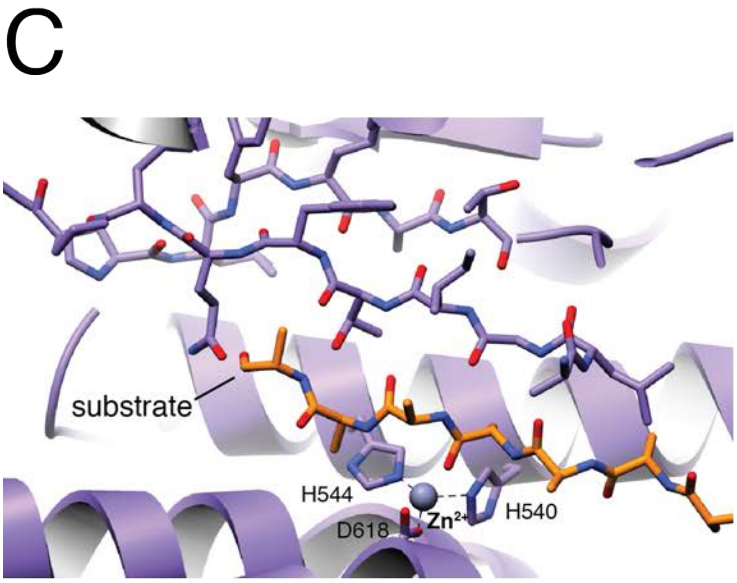
C
substrate
H544
D618
Zn2+
H540

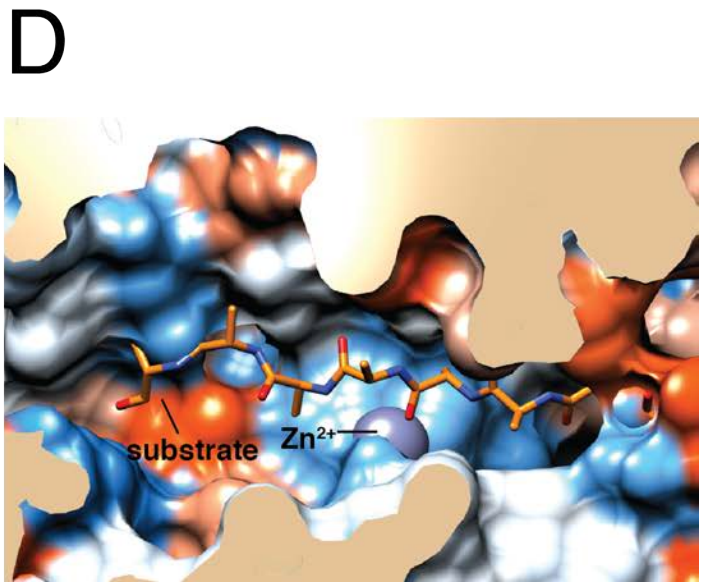
D
substrate
Zn2+

Supplementary Figure 3. Analysis of the interior of the proteolytic chamber of YME1

A) Coulombic surface potential for the interior chamber of ^{hex}YME1. Negative charges are shown in red, positive charges are shown in blue, and white shows neutral residues. This surface representation reveals that the two hexameric stacked rings formed by the AAA+ ATPase and protease domains give rise to a negatively charged proteolytic chamber interior. **B**) Molecular surface colored by hydrophobicity based on the Kyte-Doolittle scale, with hydrophilicity shown in blue and hydrophobicity in orange. This analysis reveals a very hydrophilic chamber where only a small hydrophobic patch is accessible from the interior of the chamber, and is located directly adjacent to the zinc ion (shown in yellow). **C)** Close-up view of the proteolytic active site of ATP1 subunit, with the catalytic zinc shown in grey. A poly-Alanine peptide, modeled as a β-strand, can be accommodated as an additional β-strand between β7 and the proteolytic active site, thereby positioned for cleavage. The peptide is represented as sticks in orange and the adjacent areas are depicted as sticks. **D)** The same view shown in (C), using a molecular surface representation and colored by hydrophobicity.

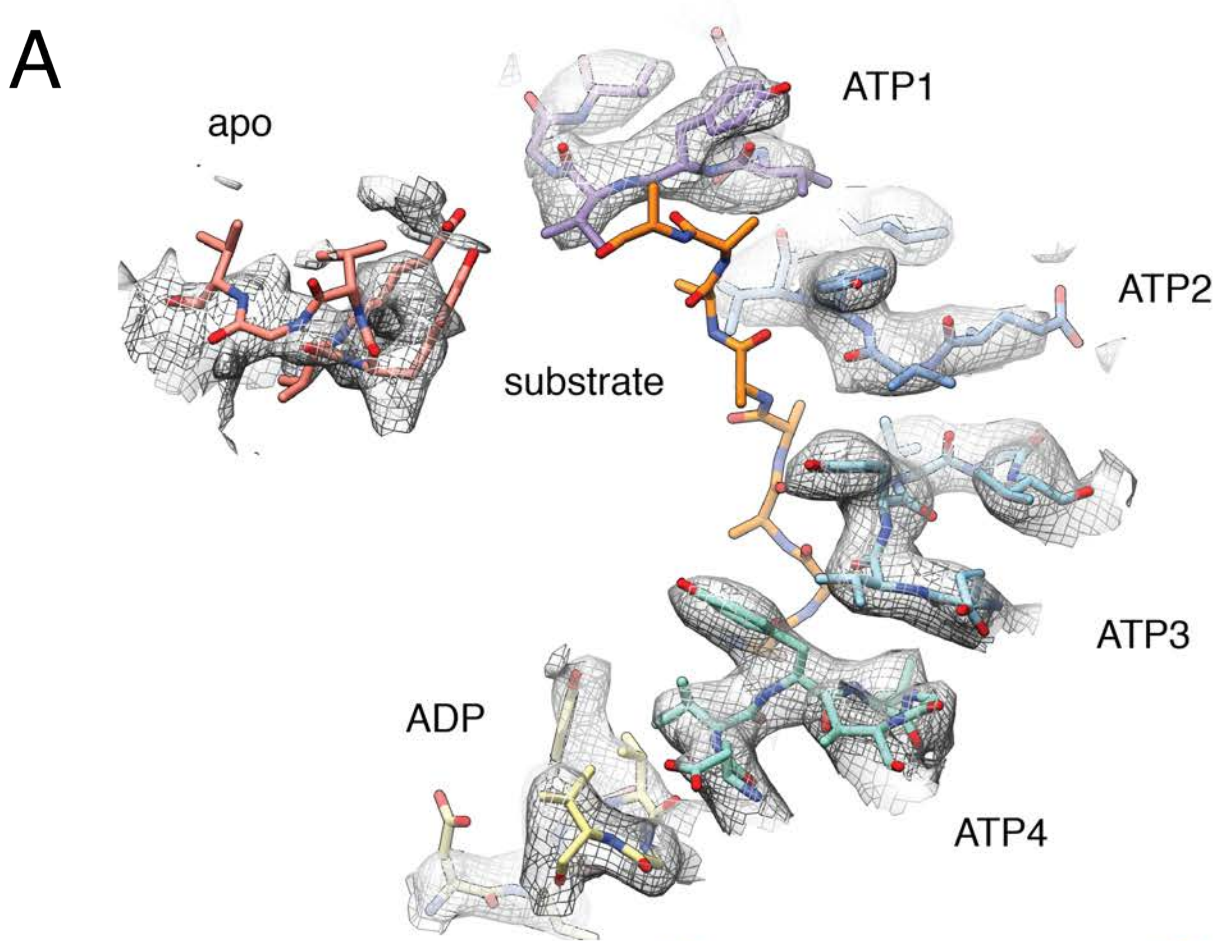
A
apo
ATP1
ATP2
substrate
ATP3
ADP
ATP4

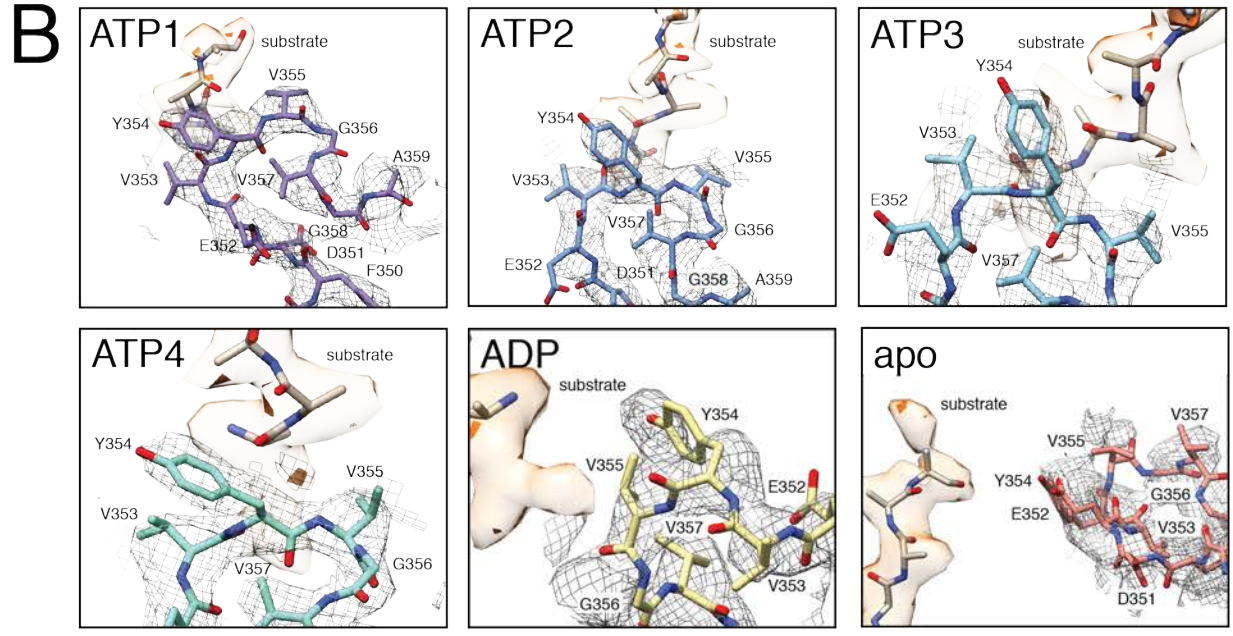
B
ATP1
substrate
V355
Y354
G356
A359
V353
V357
G358
E352
D351
F350
ATP2
substrate
Y354
V355
V353
V357
G356
E352
D351
G358
A359
ATP3
substrate
Y354
V353
E352
V355
V357
ATP4
substrate
Y354
V355
V353
V357
G356
ADP
substrate
Y354
V355
E352
V357
V353
G356
apo
substrate
V357
V355
Y354
G356
E352
V353
D351

Supplementary Figure 4. Structural details of the pore-loop 1 staircase in the presence of substrate

A) Atomic model and cryo-EM density for pore-loop 1 residues 351-357 of all subunits reveal a continuous spiral staircase organization, where pore-loop 1 of subunits ATP1-4 are well-resolved and assume an identical organization, whereas ADP and apo are less resolved and in different conformations. The Y354 of subunits ATP1-4 intercalates into the substrate (orange stick representation) every two amino acids, in a zipper-like configuration. We refer to these Tyr residues as 'intercalating'. In contrast, Y354 from the ADP subunit follows the staircase, but does not intercalate into the substrate. We refer to this Tyr as 'proximal'. Y345 from the apo subunit is does not follow the staircase, does not interact with substrate, and is poorly ordered. We refer to this Tyr as 'non-interacting'. **B**) Detailed view of pore-loop 1 from each subunit, with the substrate density shown in orange.

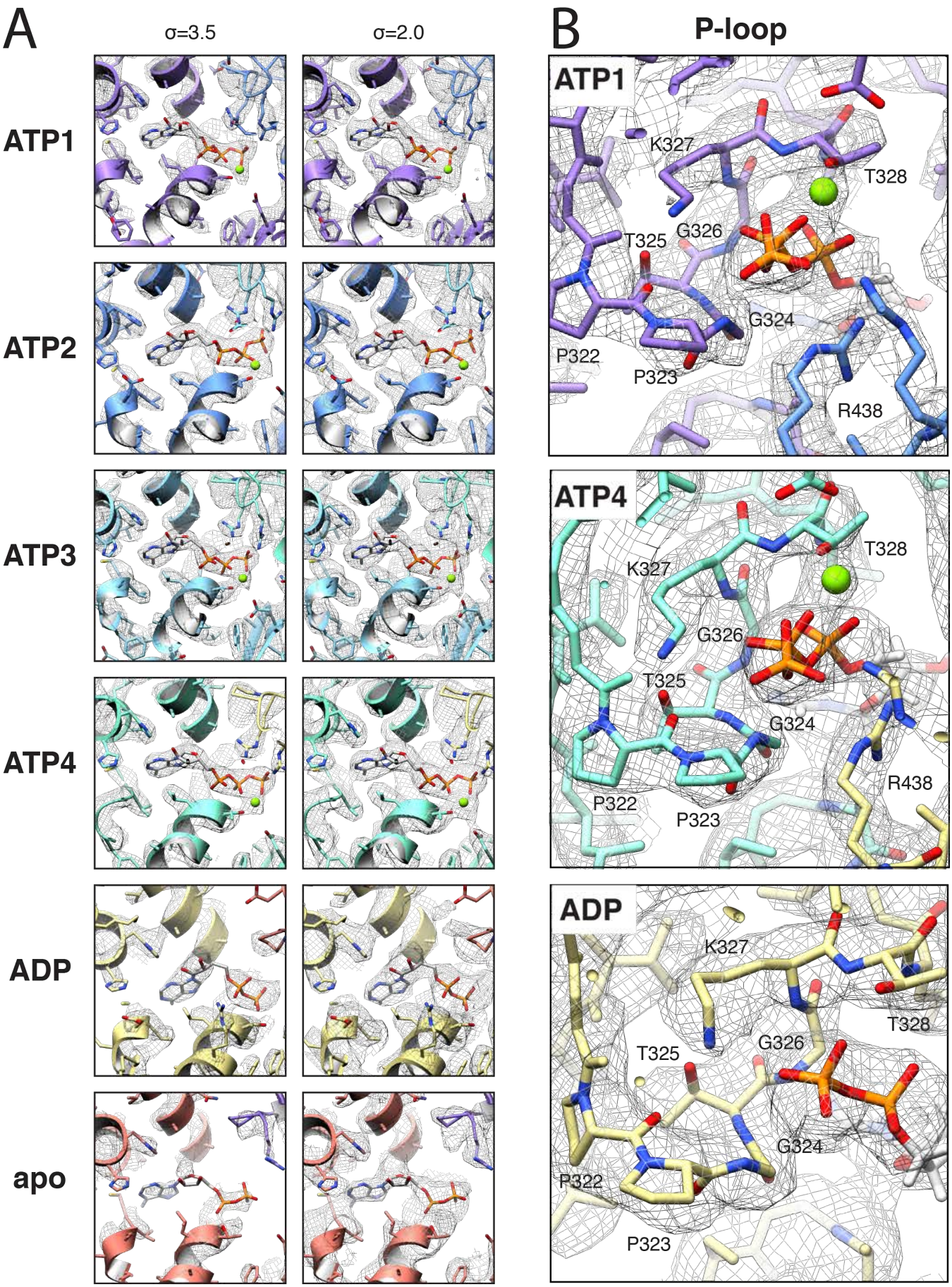
A
σ=3.5
σ=2.0
ATP1
ATP2
ATP3
ATP4
ADP
apo
B
P-loop
ATP1
K327
T328
T325
G326
G324
P322
P323
R438
ATP4
T328
K327
G326
T325
G324
R438
P322
P323
ADP
K327
T328
T325
G326
G324
P322
P323

Supplementary Figure 5. Distinct nucleotide densities in the nucleotide-binding pocket and their interaction with the P-loop residues

A) The cryo-EM density of the entire nucleotide-binding pocket within each subunit is shown, using an isosurface mesh contoured at a level of σ=3.5 (left), and σ=2 (right) enables unambiguous distinction of nucleotide density in the different subunits. ATP1, ATP2, ATP3, and ATP4 subunits all present a very strong nucleotide density corresponding to ATP coordinated by a magnesium ion. In contrast, the nucleotide density of the ADP subunit was modeled as an ADP because no density was found either a gamma phosphate or a magnesium ion. In the step subunit (red ribbon) the lower intensity of the nucleotide density is indicative of lower occupancy, indicating that the nucleotide-binding pocket of this subunit was empty in much of the dataset. Together, these data strongly suggest that three nucleotide states coexist in the substrate-bound structure, where ATP1-4 are bound to ATP, whereas ADP and apo subunits appear to represent transition states for ATP-hydrolysis/Pi release and ADP release, respectively. **B)** Atomic model and cryo-EM density of the P-loop (PPGTGKT) and the nucleotide are shown for ATP1, ATP4 and ADP subunits. The nucleotide phosphates are located within 4 Å of the P-loop backbone, which appears to interact with both ATP and ADP. These observations suggest an important role for this loop in nucleotide binding, thereby explaining the high degree of conservation of this motif among ATPases (Supplementary Figure 6).

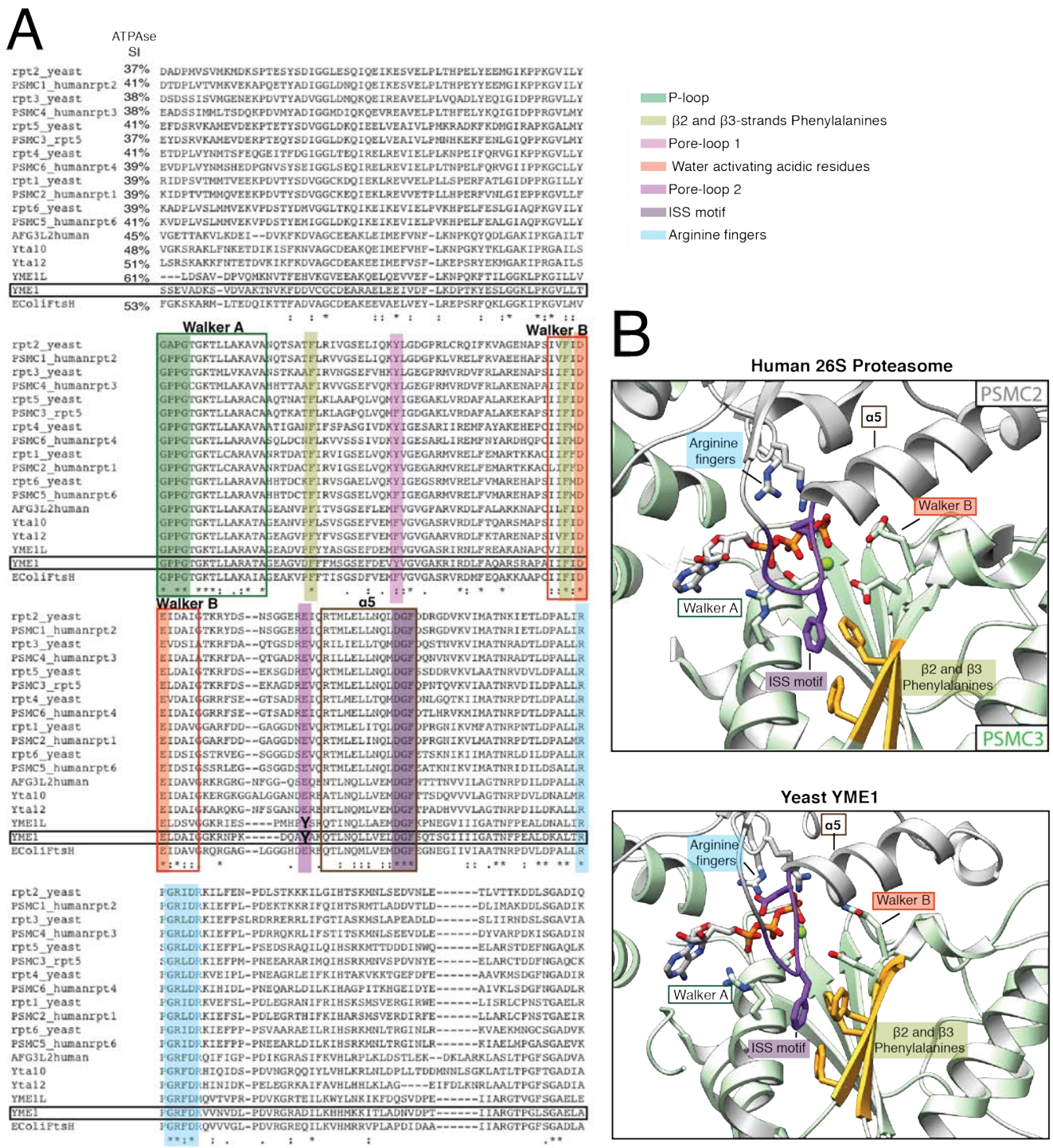

Supplementary Figure 6. Sequence homology and structural similarities between distantly related ATPases suggests mechanistic conservation.

A) ClustalW alignment (Larkin 2007) of the Uniprot sequences of the ATPase domains of YME1 with YME1 homologs (human YME1L and bacterial FtsH), paralogs (human AFG3L2, and yeast Yta10 and Yta12), as well as yeast proteasome ATPases (Rpt1-6) and human proteasome (PSMC 1-6) ATPases. This comparison shows very high sequence identity (ATPase SI) between evolutionary very distant ATPase domains (above 35% in all cases). Further analysis of the alignments strongly suggests mechanistic conservation, as we found

all key residues identified in our structure to be strictly conserved in all sequences studied: P-loop (green in Walker A motif), basic residue (dark blue in Walker A motif), aromatic residue in pore-loop 1 (light pink), β2 and β3 phenylalanines (yellow), acidic residues (orange) in Walker B motif, ISS motif (purple) and arginine fingers (light blue). Interestingly, the aromatic residue in pore-loop 2 (dark pink) is conserved in YME1 throughout eukaryotes (from yeast to human), but is a glutamic acid in all other ATPases analyzed here. This observation suggests a role of this residue that is specific to the function of YME1 and related homologs. **B)** The ATP-bound nucleotide-binding pockets of human 26S proteasome (top panel, PDBID: 5MP9 (Wehmer 2017)) and YME1 (bottom panel) contain many structurally conserved features. The pocket shown is at the interface between adjacent subunits (PSMC2 and 3 in the heterohexameric human 26S proteasome, and ATP2 and ATP3 in the yeast YME1 homohexamer). In both cases, the arginine fingers of the clockwise adjacent subunit coordinate ATP and the ISS motif extends in trans with the F interacting with β2 and β3 phenylalanines of the adjacent subunit. Other key elements of the mechanism described here are also structurally conserved, including the magnesium coordinating threonine, the Walker B acidic residues, and the position of helix σ5 with the ISS motif at its N-terminus and pore-loop 2 at its C-terminus.

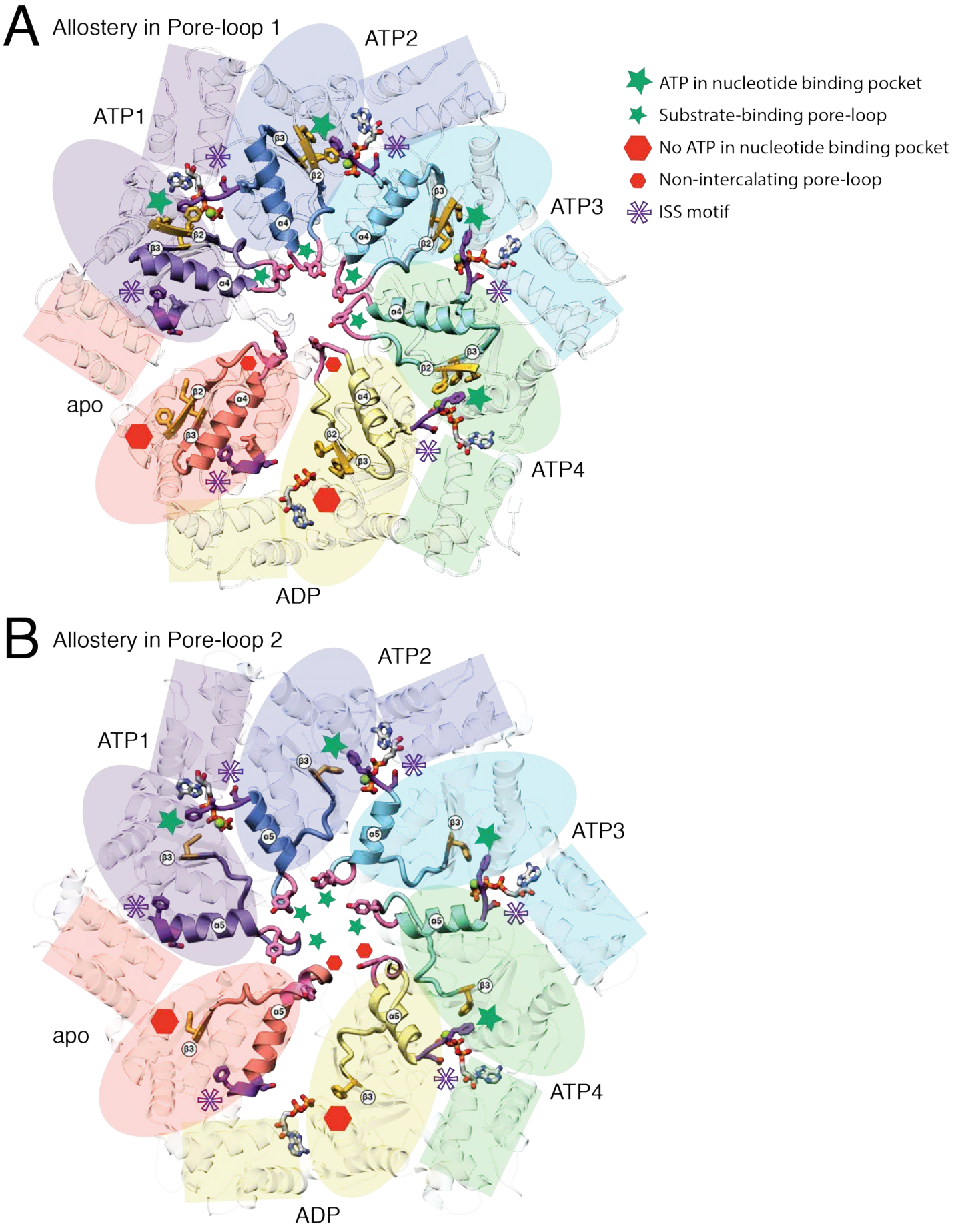
A
Allostery in Pore-loop 1
ATP2
ATP1
ATP3
apo
ATP4
ADP
ATP in nucleotide binding pocket
Substrate-binding pore-loop
No ATP in nucleotide binding pocket
Non-intercalating pore-loop
ISS motif
B
Allostery in Pore-loop 2
ATP2
ATP1
ATP3
apo
ATP4
ADP

Supplementary Figure 7. Mechanism of allostery coordinating nucleotide state to pore-loop conformation

A) Allostery linking nucleotide-state to pore loop 1. Top view of the substrate-bound YME1 hexamer with the large and small domains of each subunit represented by an ellipse and a rectangle, respectively. Residues 342-378 are highlighted and comprise the β2 strand (342-346), pore-loop 1 (352-356, pink), helix α4 (357-371), and β3 (376-380). These secondary structure elements include F342, F344 (gold in β2), F378 (gold in β3) and Y354 (pink in pore loop-1). The ISS motif (409-411) is shown in purple for every subunit. When ATP is in the nucleotide-binding pocket, the ISS motif of the clockwise adjacent subunit adopts an extended loop conformation, with its F411 interacting with F342, F344, and F378 of the ATP-bound subunit. These interactions influence the position of β2, which translates to a substrate-interacalating pore loop 1 conformation (intercalating Tyr residues). In the absence of ATP, these inter-subunit interactions are lost, altering pore loop conformation. Since the ISS motif of the ADP-containing subunit interacts with the ATP4 subunit, the pore loop of the ADP subunit remains in proximity of the substrate (proximal Tyr). The nucleotide-free subunit, on the other hand, is disconnected from both neighboring subunits, resulting in a dislocation of the entire ATPase domain and its pore loop, from the spiral staircase (non-interacting Tyr). **B)** Pore loop 2 rearrangements are analogous to pore loop 1. Interaction of the ISS motif with the β3 phenylalanine translates to a substrate-interacting conformation of pore loop 2. When ATP is not present in the counter-clockwise adjacent subunit, the ISS motif folds to become a C-terminal extension of helix σ5. In the apo subunit, loss of interaction with both neighboring protomers results in a folding of the pore loop to become an N-terminal extension of helix σ5. Together, these conformational rearrangements give rise to a continuous nucleotide-dependent inter-subunit coordination network.

A

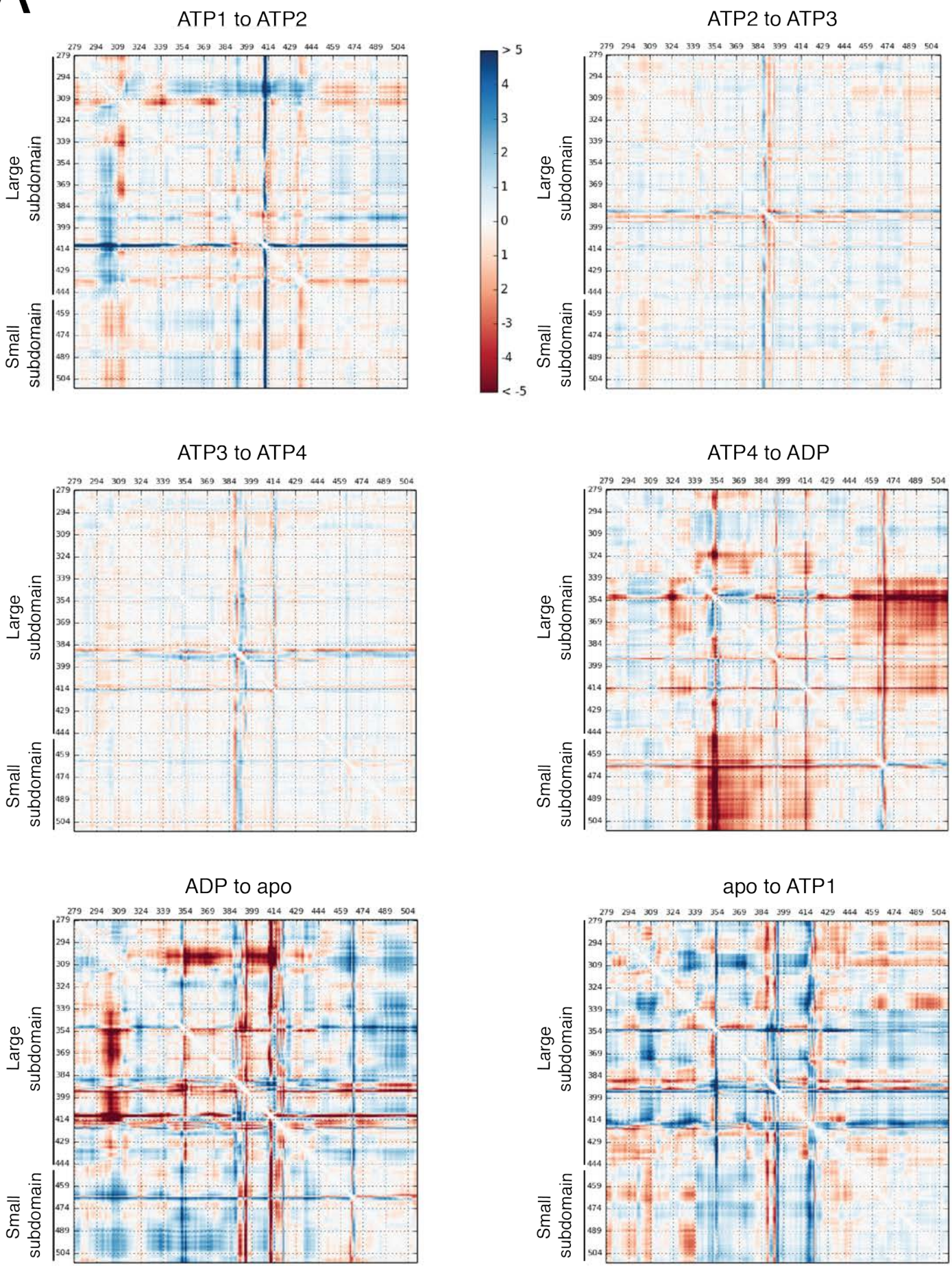
ATP1 to ATP2
ATP2 to ATP3
ATP3 to ATP4
ATP4 to ADP
ADP to apo
apo to ATP1
Large subdomain
Small subdomain
279 294 309 324 339 354 369 384 399 414 429 444 459 474 489 504
> 5
4
3
2
1
0
1
2
-3
-4
< -5

B

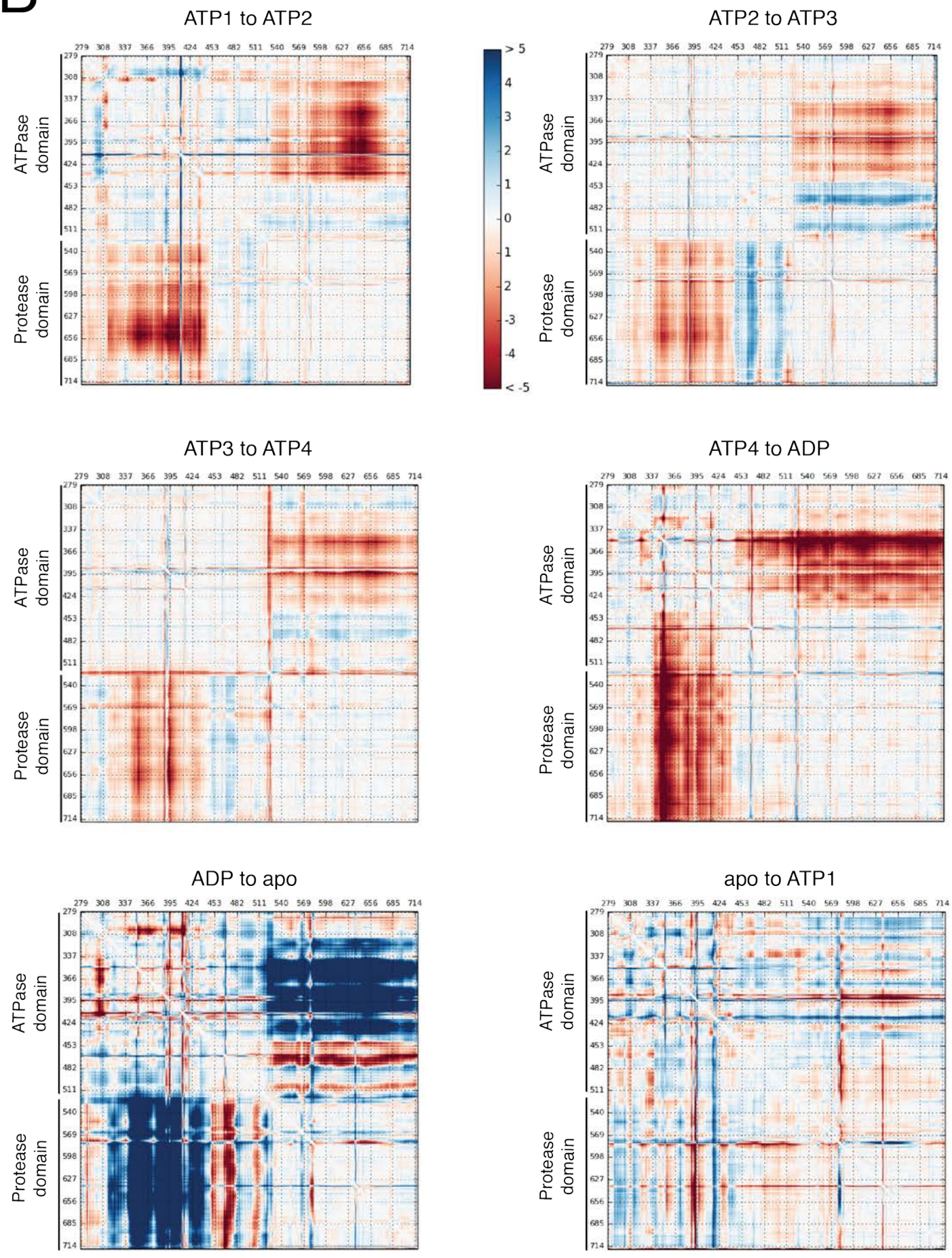
ATP1 to ATP2
ATP2 to ATP3
ATP3 to ATP4
ATP4 to ADP
ADP to apo
apo to ATP1
ATPase domain
Protease domain
279 308 337 366 395 424 453 482 511 540 569 598 627 656 685 714
> 5
4
3
2
1
0
1
2
-3
-4
< -5

Supplementary Figure 8. Analysis of the conformational changes between ATPase domains of adjacent subunits in the substrate-bound hexamer.

A) Pairwise difference distance matrices comparing the position of the Cα of each amino acid to the Cα of all other amino acids in the clockwise adjacent subunit for the ATPase domain. The amino acids whose Cα are closer to one another in the clockwise adjacent subunit are assigned a negative value, and colored increasingly red. Increased distances between amino acids result in positive values and colored increasingly blue. All values are measured in Å, and distances are capped at 5 Å in either direction. These distance matrices clearly illustrate major nucleotide dependent changes, including rigid body rotations that affect entire domains, as well as positional changes of the ISS motif. Notably, the ATPase subunits do not differ substantially from one another when bound to ATP, and the largest rearrangements occur upon ATP hydrolysis and nucleotide release. **B**) Pairwise difference distance matrices comparing the position of the Cα of each amino acid to the Cα of all other amino acids in the clockwise adjacent subunit the entire subunit, including the protease domain. These matrices show that the ATPase domain moves progressively closer to the protease domain through the ATP-bound conformations, until it reaches the ADP conformation. As the ADP subunit transitions to the apo conformation, the ATPase subunit moves significantly away from the protease domain.

Supplementary Table 1. Data collection, reconstruction, and model refinement statistics

	^{hex}YME1^{WB}
Data collection	
Microscope	Titan Krios
Voltage (keV)	300
Nominal magnification*	29,000x
Exposure navigation	Image Shift
Electron dose (e^{-} Å^{-2})	60
Dose rate (e^{-}/pixel/sec)	8
Detector	K2 Summit
Pixel size (Å)*	1.03
Defocus range (μm)	1.2 - 2.5
Micrographs	6098
Total extracted particles (no.)	2,285,499
Refined particles (no.)	1,792,531
Reconstruction	
Final particles (no.)	62,917
Symmetry imposed	C1
Resolution (global)	
FSC 0.5 (masked)	3.9 Å
FSC 0.143 (masked)	3.4 Å
Applied B-factor (Å^{2})	-98.86
Refinement**	
Protein residues	2628
Ligands	18
Map Correlation Coefficient	
Local	0.8282
Bond lengths	0.008
Bond angles (°)	0.84
Ramachandran (%)	
Outliers	0.08
Allowed	7.88
Favored	92.05
Poor rotamers (%)	0
MolProbity score	1.792
Clashscore (all atoms)	5.66
Mean per-residue Cα RMSD (Å)	0.54
Per-residue Ca RMSD range (Å)	0.02-4.5
EMRinger Score (Barad 2015)	3.6

*Calibrated pixel size at the detector

Supplementary References

Barad, B. A., N. Echols, R. Y. Wang, Y. Cheng, F. DiMaio, P. D. Adams and J. S. Fraser (2015). "EMRinger: side chain-directed model and map validation for 3D cryo-electron microscopy." Nat Methods **12**(10): 943-946.

Cardone, G., J. B. Heymann and A. C. Steven (2013). "One number does not fit all: mapping local variations in resolution in cryo-EM reconstructions." J Struct Biol **184**(2): 226-236.

Herzik, M. A., J. S. Fraser and G. C. Lander (2017). "A multi-model approach to assessing local and global cryo-EM map quality." bioRxiv.

Larkin, M. A., G. Blackshields, N. P. Brown, R. Chenna, P. A. McGettigan, H. McWilliam, F. Valentin, I. M. Wallace, A. Wilm, R. Lopez, J. D. Thompson, T. J. Gibson and D. G. Higgins (2007). "Clustal W and Clustal X version 2.0." Bioinformatics **23**(21): 2947-2948.

Scheres, S. H. (2012). "RELION: implementation of a Bayesian approach to cryo-EM structure determination." J Struct Biol **180**(3): 519-530.

Wehmer, M., T. Rudack, F. Beck, A. Aufderheide, G. Pfeifer, J. M. Plitzko, F. Forster, K. Schulten, W. Baumeister and E. Sakata (2017). "Structural insights into the functional cycle of the ATPase module of the 26S proteasome." Proc Natl Acad Sci U S A **114**(6): 1305-1310.